Modeling Earth Albedo for Satellites in Earth Orbit.

Dan D. V. Bhanderi *

Aalborg University, Fredrik Bajers Vej 7C, DK-9220 Aalborg Oest, Denmark

Thomas Bak †

Danish Institute of Agricultural Sciences, Schüttesvej 17, DK-8700 Horsens, Denmark

Many satellite are influenced by the Earth's albedo, though very few model schemes exist, in order to predict this phenomenon. Earth albedo is often treated as noise, or ignored completely. When applying solar cells in the attitude hardware, Earth albedo can cause the attitude estimate to deviate with as much as 20 deg. Digital Sun sensors with Earth albedo correction in hardware exist, but are expensive. In addition, albedo estimates are necessary in thermal calculations and power budgets. We present a modeling scheme based on Earth reflectance, measured by NASA's Total Ozone Mapping Spectrometer, in which the Earth Probe Satellite has recorded reflectivity data daily since mid 1996. The mean of these data can be used to calculate the Earth albedo given the positions of the satellite and the Sun. Our results show that the albedo varies highly with the solar angle to the satellite's field of view, and that the longitude of the satellite position is significant to the model output. The results also show that the calculated albedo is generally lower than it would be expected based only on the reflectivity data.

Nomenclature

A_c = Cell area
α_{sat} = Angle to satellite from grid point
α_{Sun} = Angle of incident irradiance on cell
c = Speed of light in vacuum
$\boldsymbol{D}$ = Set of grid points
$\Delta\phi_g$ = Angular resolution in latitude
$\Delta\theta_g$ = Angular resolution in longitude
$\boldsymbol{\Phi}$ = Set of latitude grid points
E_a = Total albedo
E_{AM0} = Incident air mass zero solar irradiance at 1AU
E_{bb} = Black body spectrum
E_c = Cell albedo irradiance
E_r = Reflected irradiance
E_{sat} = Reflected irradiance at satellite distance
ϕ_g = Polar angle of grid point
h = Planck's constant
i = Current
k = Boltzmann's constant
λ = Wavelength
$\hat{\boldsymbol{n}}_c$ = Cell normal vector
P_c = Incident radiant flux density
P_r = Reflected radiant flux
$\boldsymbol{q}_0$ = Initial quaternion

*Assistant Professor, Department of Control Engineering.
†Head of Research Group, Department of Automation and System Technology.

r_{E} = Earth mean radius
$\boldsymbol{r}_{\mathrm{sat}}$ = Satellite position vector
r_{Sun} = Sun mean radius
$\boldsymbol{r}_{\mathrm{Sun}}$ = Sun position vector
ρ = Reflectivity
T = Black body temperature
$\boldsymbol{\Theta}$ = Set of longitude grid points
θ_{g} = Azimuth angle of grid point
$\boldsymbol{V}_{\mathrm{sat}}$ = Set of grid points in satellite FOV
$\boldsymbol{V}_{\mathrm{Sun}}$ = Set of sunlit grid points
$\boldsymbol{\omega}_0$ = Initial angular velocity

I. Introduction

Earth albedo is relevant for practically all Earth orbiting satellites. The amount of solar radiation reflected by the Earth towards a satellite, influences the power generated by solar panels, generates radiation torques, affects the thermal design, and is measured by horizon sensors to estimate satellite attitude.[1–3] Albedo is typically treated as noise to the attitude determination system (ADS). The albedo disturbance is either filtered out statistically in Kalman algorithms,[4,5] which is possible when used with magnetometers, or it can be measured using albedo sensors.[6] Digital Sun sensors are also available, which are mostly insensitive to albedo light by implementing an active pixel array instead of solar cells.[7] Some configurations result in errors in the least significant bits of the digital Sun sensors.[8] Some algorithms simply rely on protection of stray light in the sensor hardware.[9]

The work in this paper is a study of advanced albedo modeling for use in off-line attitude algorithms. The algorithm will be implemented for the AAUSAT-II satellite.[10] The satellite is in the pico satellite class, i.e. 1.0kg total mass, limiting the amount of sensor hardware. Typical hardware solutions for satellites of this class are a magnetometer combined with Sun sensors or merely using the solar panels.[4,11,12] Sun sensors, however, not only measure the direct solar radiance, but also the Earth albedo. This can decrease accuracy of the Sun pointing determination by more than 20 deg.[13]

A significant research effort in Earth albedo has been conducted in the geophysical and meteorological research communities (see e.g.[14–16]). The results of these studies are mainly focused on spectral distributions of absorbance and reflectivity of the atmosphere and different Earth surface scenarios. Earth observations by satellites and high altitude aircrafts and balloons, have been used to acquire accurate data of the Earth reflectance and radiance.[17] These results can be applied in the calculation of Earth albedo received by a satellite in the vicinity of Earth.

The work done in ([13]) is modeling albedo by observing the reflectance of the Earth's surface. The results are based on data from the Total Ozone Mapping Spectrometer (TOMS) project. The data are simplified by merging the reflectivity data for a given latitude. In this paper, we calculate the expected value of the albedo based on the full data set from the TOMS project, showing that the longitude in some cases can double the model output.

Section II presents the reflectivity data, measured by the Earth Probe satellite, on which the albedo calculations are based, followed by a principal description of the albedo model and the equations used to calculate the albedo. Section III presents some representative results of the model. The matlab files are released as a toolbox for Matlab/Simulink and are available online.[18]

II. Albedo Model

The modeling of the Earth albedo is based on the reflectivity data, measured by the Earth Probe Satellite for the TOMS project. The data are available online at the TOMS website.[19] The satellite data are given in a resolution of $\Delta\phi_{\mathrm{g}} = 1$ deg latitude times $\Delta\theta_{\mathrm{g}} = 1.25$ deg longitude, i.e. 180×288 data points. The 2D data space $\boldsymbol{D}$ is defined as a grid of data points $\boldsymbol{\Phi} \times \boldsymbol{\Theta}$, where

$$\boldsymbol{\Phi} = [0, \Delta\phi_{\mathrm{g}}, 2\Delta\phi_{\mathrm{g}}, ..., 179\Delta\phi_{\mathrm{g}}]\,, \tag{1}$$

$$\boldsymbol{\Theta} = [0, \Delta\theta_{\mathrm{g}}, 2\Delta\theta_{\mathrm{g}}, ..., 287\Delta\theta_{\mathrm{g}}]\,. \tag{2}$$

Each data point $(\phi_g, \theta_g) \in \boldsymbol{D}$ is the mean reflectance of a cell, $\phi_g \pm \Delta\phi_g/2$ and $\theta_g \pm \Delta\theta_g/2$, on the Earth surface.

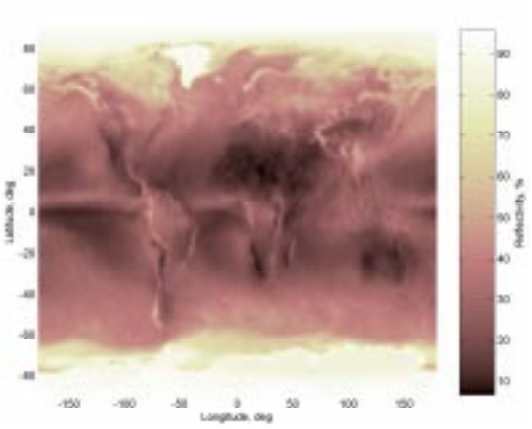

Figure 1. Plot of TOMS mean reflectivity data recorded from January 1 to December 31, 2001.

The TOMS Earth Probe data are available daily, but fluctuate because of changes in cloud coverage and seasonal changes. A mean reflectivity and standard deviation of the data for the year 2001 are calculated. The result is shown in Fig. 1. The standard deviation of the data is shown in Fig. 2. The plots show that there is high reflectivity over the poles, which can be expected due to the polar ice caps, and low reflectivity around the Equator. The standard deviation is higher around the Equator due to changing cloud coverage. Over the poles, the icy surface ensures high reflectivity regardless of cloud coverage. The data suggest an average Earth reflectivity of 30.40%, which is consistent with the literature.[3,17] The average is calculated by weighting each reflectivity measurement with respect to the area of the associating cell at the measurement grid point.

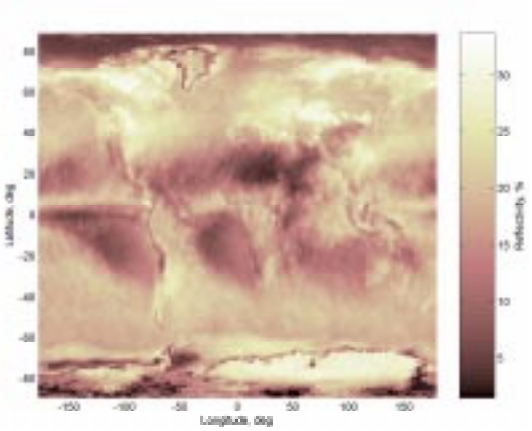

Figure 2. Plot of standard deviation of the TOMS reflectivity data recorded from January 1 to December 31, 2001.

The principle of the modeling scheme is outlined in Fig. 3. The incident solar irradiance E_{AM0} reaches the cell at grid point (ϕ_g, θ_g), at an incident angle of α_{Sun} to the cell normal $\hat{\boldsymbol{n}}_c$. The angle of incidence defines density of the incident irradiance on the cell. The subscript AM0 states that the irradiance has passed through zero air mass.[20] It is assumed that the effect of air mass does not change the spectrum apart from the changes recorded in the reflectivity data at 360nm. The amount of radiant flux reflected by the cell is given by the irradiance and the area of the cell, $A_c(\phi_g)$. The Earth albedo contribution of the cell, E_c, reaches the satellite, and the density of the radiant flux is dependent on the angle α_{sat}.

The incident AM0 solar irradiance is modeled by a black body spectrum with a surface temperature of

$5777K$.[3] The spectrum $E_{\mathrm{bb}}(\lambda, T)$ is calculated using Planck's Law

$$E_{\mathrm{bb}}(\lambda, T) = \frac{2\pi c^2 h}{\lambda^5 \left(e^{ch/(k\lambda T)}\right)}, \tag{3}$$

where c is the velocity of light, h is Planck's constant, k is Boltzmann's constant, λ is the wavelength, and T the temperature. The total incident solar irradiance is found by integrating $E_{\mathrm{bb}}(\lambda, T)$ over all wavelengths. Accounting for the Sun Earth distance using the Inverse Square Law yields

$$E_{\mathrm{AM0}} = \frac{r_{\mathrm{Sun}}^2}{(1\mathrm{AU})^2} \int_{-\infty}^{\infty} E_{\mathrm{bb}}(\lambda, T)\, d\lambda = 1366.5\mathrm{W/m}^2, \tag{4}$$

where r_{Sun} is the Sun mean radius. The resulting AM0 irradiance is in accordance with satellite measurements.[21] In the albedo model, only E_{AM0} is used. It may be assumed that the Earth albedo spectrum has the same distribution as the AM0 irradiance.[3] The Earth absorbed solar irradiance, which is radiated back into space is not included in the model, since a typical solar cell does not absorb radiance at wavelengths longer than 2μm (see e.g.[22]). The Earth radiance, modeled as a 288K black body spectrum model, peaks at 10μm and less than $4 \cdot 10^{-8}\%$ of the energy is at wavelengths shorter than 2μm.

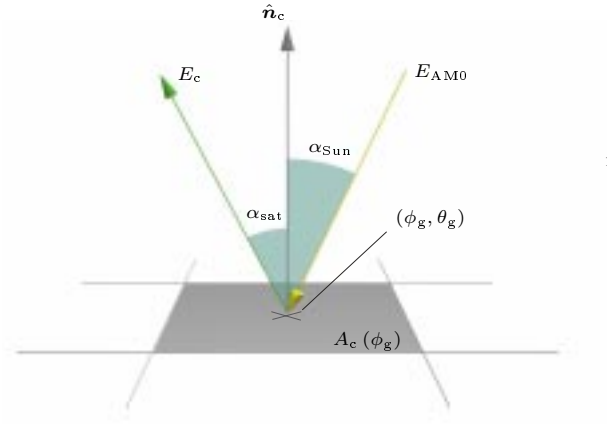

Figure 3. ***Earth albedo modeling principle. The incoming solar AM0 irradiance is reflected by a cell.***

The incident solar irradiance hits a cell on the Earth's surface. The amount of energy reflected by the cell depends on the cell area $A_{\mathrm{c}}(\phi_{\mathrm{g}})$, given by

$$A_{\mathrm{c}}(\phi_{\mathrm{g}}) = \theta_{\mathrm{g}} r_{\mathrm{E}}^2 \left(\cos\left(\phi_{\mathrm{g}} - \frac{\Delta\phi_{\mathrm{g}}}{2}\right) - \cos\left(\phi_{\mathrm{g}} + \frac{\Delta\phi_{\mathrm{g}}}{2}\right)\right), \tag{5}$$

where r_{E} is the Earth mean radius.

The incoming irradiance is equal to the solar AM0 irradiance, multiplied by a cosine term dependent on the incident angle α_{Sun}, which is the angle between the cell normal $\hat{\boldsymbol{n}}_{\mathrm{c}}$ and the Sun LOS vector $\hat{\boldsymbol{r}}_{\mathrm{Sun}}$. The intensity of the incoming irradiance decreases as the angle of attack increases. This is equivalent to the observed cell area along the Sun LOS vector. The incident radiant flux $P_{\mathrm{c}}(\phi_{\mathrm{g}}, \theta_{\mathrm{g}})$ on a single cell at latitude with polar angle ϕ_{g} is given by

$$P_{\mathrm{c}}(\phi_{\mathrm{g}}, \theta_{\mathrm{g}}) = E_{\mathrm{AM0}} A_{\mathrm{c}}(\phi_{\mathrm{g}}) \left\{\hat{\boldsymbol{r}}_{\mathrm{Sun}}^{\mathrm{T}} \hat{\boldsymbol{n}}_{\mathrm{c}}\right\}_0^{\infty}. \tag{6}$$

The notation $\{\cdot\}_0^{\infty}$ denotes lower saturation of zero, since incident angles higher than $\pi/2$ result in zero, and not negative, radiant flux. Note that the dependency on the grid point is left out for vectors in order to preserve readability. The reflection on the Earth surface is assumed to be Lambertian. Lambertian surfaces have a diffuse reflection, which is independent on the incident angle of the incoming radiance, and look evenly illuminated regardless of the viewing angle.[23] The reflected radiant flux $P_{\mathrm{r}}(\phi_{\mathrm{g}}, \theta_{\mathrm{g}})$ is calculated as a fraction, $\rho(\phi_{\mathrm{g}}, \theta_{\mathrm{g}})$, of the incoming radiant flux in Eq. (6)

$$P_{\mathrm{r}}(\phi_{\mathrm{g}}, \theta_{\mathrm{g}}) = \rho(\phi_{\mathrm{g}}, \theta_{\mathrm{g}})\, P_{\mathrm{c}}(\phi_{\mathrm{g}}, \theta_{\mathrm{g}}), \tag{7}$$

where $\rho(\phi_g, \theta_g)$ is the mean reflectivity at grid point $(\phi_g, \theta_g) \in \boldsymbol{D}$.

The amount of Earth albedo from a single cell, seen from the satellite, depends on the distance to the satellite and the angle between the cell normal and the satellite LOS vector from the grid point, $\hat{\boldsymbol{r}}_{sat}$. The irradiance $E_r(\phi_g, \theta_g)$ of the cell, when assuming Lambertian reflectivity, is related to the radiant exitance by[23]

$$E_r(\phi_g, \theta_g) = \frac{P_r(\phi_g, \theta_g)}{\pi}. \tag{8}$$

The Inverse Square Law states that the intensity of the irradiance decreases with the square of the distance from the grid point to the satellite, which is written as

$$E_{sat}(\phi_g, \theta_g) = \frac{E_r(\phi_g, \theta_g)}{||\hat{\boldsymbol{r}}_{sat}||^2}. \tag{9}$$

Finally the irradiance at the satellite depends on the visible area of the cell surface seen from the satellite. The visible area is related to α_{sat} by the cosine function. This relationship, combined with Eqs. (7) and (8), results in an expression of the Earth albedo irradiance $E_c(\phi_g, \theta_g)$ from a single cell, given by

$$E_c(\phi_g, \theta_g) = \frac{P_r(\phi_g, \theta_g)\left\{\hat{\boldsymbol{r}}_{sat}^T \hat{\boldsymbol{n}}_c\right\}_0^\infty}{\pi ||\hat{\boldsymbol{r}}_{sat}||^2}. \tag{10}$$

The full Earth albedo model is expressed as

$$E_c(\phi_g, \theta_g) = \begin{cases} \frac{\rho(\phi_g,\theta_g) E_{AM0} A_c(\phi_g) \hat{\boldsymbol{r}}_{Sun}^T \hat{\boldsymbol{n}}_c \hat{\boldsymbol{r}}_{sat}^T \hat{\boldsymbol{n}}_c}{\pi ||\hat{\boldsymbol{r}}_{sat}||^2} & \text{if } (\phi_g, \theta_g) \in \boldsymbol{V}_{Sun} \cap \boldsymbol{V}_{sat} \\ 0 & \text{else} \end{cases}. \tag{11}$$

The sets $\boldsymbol{V}_{Sun} \subset \boldsymbol{D}$ and $\boldsymbol{V}_{sat} \subset \boldsymbol{D}$ are the grid points visible from the Sun and satellite, respectively, i.e. $\boldsymbol{V}_{Sun} \cap \boldsymbol{V}_{sat}$ is the set of sunlit grid points visible from the satellite, which are necessary conditions for a cell to reflect solar irradiance to the satellite. Note that the vectors $\hat{\boldsymbol{n}}_c$, $\boldsymbol{r}_{Sun}$, and $\boldsymbol{r}_{sat}$ are functions of ϕ_g and θ_g.

The output of the albedo model is $E_c(\phi_g, \theta_g)$ from the cells at all grid points, i.e. a 180×288 matrix. This result allows for incident angular dependency, when calculating incident irradiance on e.g. solar panels. The irradiance on the solar panel decreases when the angle between the solar panel normal and the incident irradiance vector increases. The total albedo irradiance E_a at the satellite position may be calculated as the sum of irradiances from all cells

$$E_a = \sum_{\boldsymbol{V}_{Sun} \cap \boldsymbol{V}_{sat}} E_c(\phi_g, \theta_g). \tag{12}$$

III. Results

In this section we present the results of the albedo model. First an example of the model output is presented and a total coverage calculation is done. Secondly model outputs for multiple calculations are presented to show dependency on longitude and altitude. Finally the model is applied in a simple attitude estimation simulator.

A. Albedo Model

Fig. 4 shows the conditions for the albedo calculations. The top plot shows the satellite's FOV. Plot (a) shows the coordinates of the satellite, which, in spherical coordinates, are

$$\boldsymbol{r}_{sat} = \begin{bmatrix} -\pi/2\text{rad} \\ \pi/3\text{rad} \\ 7171\text{km} \end{bmatrix}, \tag{13}$$

equivalent to 90 deg West and 30 deg North at an altitude of 800km. The Sun's coordinates are

$$\boldsymbol{r}_{Sun} = \begin{bmatrix} 0\text{rad} \\ 1.17\text{rad} \\ 1\text{AU} \end{bmatrix}, \tag{14}$$

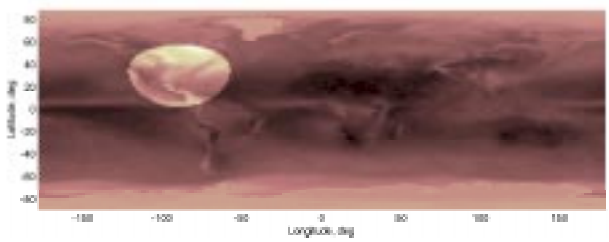

(a) Satellite FOV

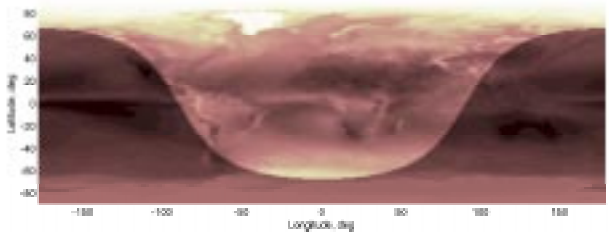

(b) Solar FOV

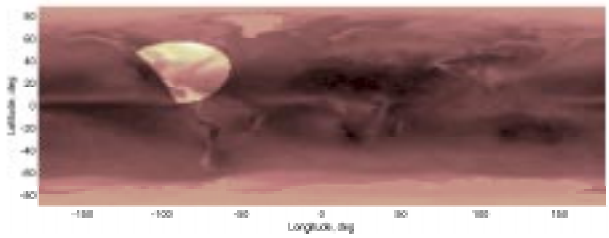

(c) Sunlit satellite FOV

Figure 4. Parameters to the albedo calculation. a) shows the satellite FOV, $V_{\mathbf{sat}}$, b) shows the Sun's FOV, $V_{\mathbf{Sun}}$, and c) shows the intersection of the two, $V_{\mathbf{sat}} \cap V_{\mathbf{Sun}}$. It is seen that the satellite is over North America at dawn.

which is at the Greenwich Meridian and 23 deg North, shown in plot (b). This means that the satellite is at an altitude of 800km over the state of Louisiana at dawn in midsummer. Plot c) shows the intersection of (a) and (b).

The albedo algorithm returns an array of same resolution as the Earth Probe reflectivity data. Each element in the array, represents the albedo contribution from a single cell. The result is shown in Fig. 5. Directional information is maintained, since the LOS vector to each grid point in the output array is known. The total albedo at the satellite, can be calculated by summing up all elements in the array. This indicates an albedo of 73.5W/m^2. This is equivalent to 5.4% of the incident solar irradiance. For comparison, the same albedo has been calculated for an altitude of 500km, which yields a total albedo of 82.5W/m^2 or 6.0%. The albedo is expected to be low, since the FOV of the satellite is partially on the night side of Earth, and over an area of generally low reflectivity.

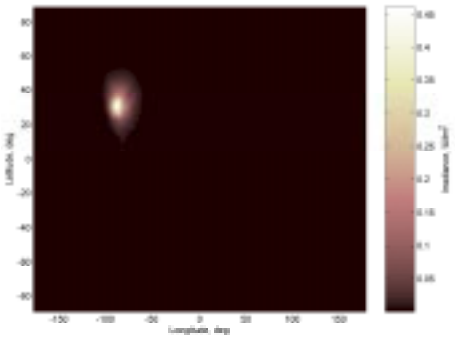

Figure 5. Result of albedo calculation given the conditions in Fig. 4.

Given specific time, the position of the Sun is constant, and the total albedo at every satellite position at a single altitude, may be calculated. This gives a instantaneous total coverage illustration of the Earth albedo. The position of the Sun is

$$\boldsymbol{r}_{\text{Sun}} = \begin{bmatrix} 0\text{rad} \\ 1.17\text{rad} \\ 1\text{AU} \end{bmatrix}, \tag{15}$$

which gives the Earth visibility shown in Fig. 6. The result of the albedo calculation, given a satellite altitude of 800km, is shown in Fig. 7. The data show that the albedo near the North Pole is 21%, and decreases moving away from the pole, and of course moving towards the shadow side of the Earth.

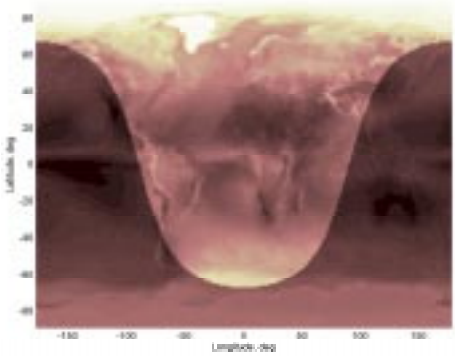

Figure 6. Solar FOV of total albedo calculation at all satellite positions.

It is often assumed that the maximum albedo is observed over the poles, due to the constant ice coverage. This has been investigated using the Earth albedo model. Due to the high angle to the Sun, the albedo is

33.8% directly over the South Pole and 36.7% over the North Pole, during local summer. From Fig. 7, the maximum albedo of approximately 49% is observed over Greenland during local summer at noon. This is due to Greenland's large ice coverage, which has a low angle to the Sun during summertime, compared to the polar regions. The Earth albedo at local winter over Greenland at noon is 36.7%.

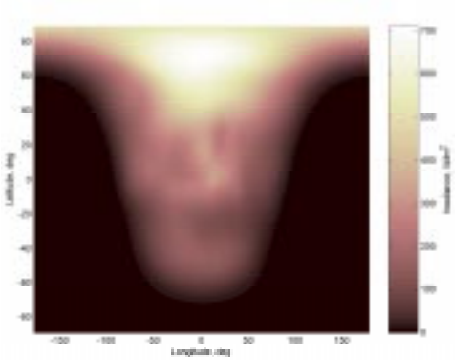

Figure 7. Total albedo at all satellite positions at an altitude of 800km, given a solar FOV shown in Fig. 6.

B. Longitude Dependency

It is known that the reflectivity data is strongly dependent on the latitude. It is sometimes assumed that the longitude dependency can be disregarded. This is investigated below.

The albedos of two sub-solar satellite positions have been calculated. The positions are equal in latitude and separated by 90 deg longitude. The input parameters of the first albedo calculation are

$$\boldsymbol{r}_{\text{sat}} = \begin{bmatrix} -\pi/2\text{rad} \\ 1.17\text{rad} \\ 6871\text{km} \end{bmatrix}, \qquad \boldsymbol{r}_{\text{Sun}} = \begin{bmatrix} -\pi/2\text{rad} \\ 1.17\text{rad} \\ 1\text{A.U.} \end{bmatrix}, \tag{16}$$

which are equivalent to 90 deg West and 23 deg North. The satellite is at an altitude of 500km, with the Sun directly above. In this case the albedo is calculated to be 356W/m^2 or 26.1%. The input parameters of the second albedo calculation are

$$\boldsymbol{r}_{\text{sat}} = \begin{bmatrix} 0\text{rad} \\ 1.17\text{rad} \\ 6871km \end{bmatrix}, \qquad \boldsymbol{r}_{\text{Sun}} = \begin{bmatrix} 0\text{rad} \\ 1.17\text{rad} \\ 1\text{A.U.} \end{bmatrix}, \tag{17}$$

which are the same as above except at the Greenwich Meridian, i.e. 90 deg East of the satellite and Sun positions of the first calculation. In this case the albedo is 187W/m^2 or 13.7%, which is almost half the albedo at 90 deg West. This shows a significant dependency on longitude of the Earth albedo.

C. Altitude Dependency

The Earth albedo is expected to decrease with the satellite altitude. In order to show this, the albedo is calculated with constant Sun and satellite directions, and varying the altitude of the satellite between 200km and 2000km. The Sun position is constant at

$$\boldsymbol{r}_{\text{Sun}} = \begin{bmatrix} 0\text{rad} \\ 1.17\text{rad} \\ 1\text{A.U.} \end{bmatrix}, \tag{18}$$

and the satellite position is sub-solar. The result of 50 albedo calculations at altitudes between 200km and 2000km is shown in Fig. 8. The calculations indicate that the albedo decreases from 15.3% at 200km to 10.5% at 2000km.

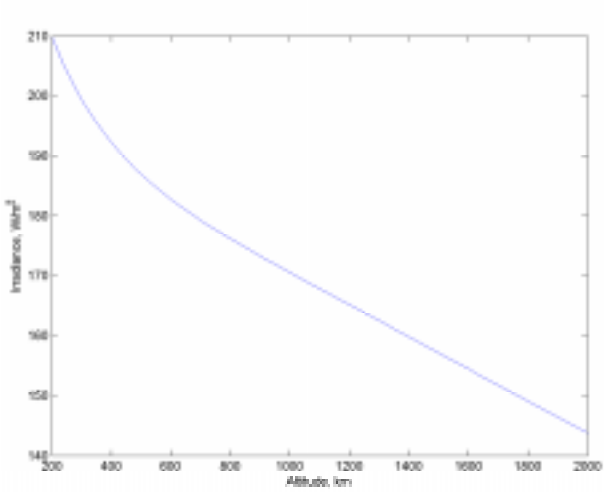

Figure 8. ***Total Earth albedo at constant sub-solar satellite position at altitudes from 200km to 2000km at Greenwich Meridian and 23 deg North.***

D. Albedo Corrected Estimation

The albedo model is applied in a simple simulation of a single orbit of the AAU CubeSat. The AAU CubeSat is a 10cm $\times$ 10cm $\times$ 10cm cubical satellite, which was launched by Aalborg University on June 30, 2003, into a Sun-synchronous orbit with an inclination of 98.7 deg. The initial conditions of the satellite are

$$\boldsymbol{q}_0 = \begin{bmatrix} 0 \\ 0 \\ 0 \\ 1 \end{bmatrix}, \qquad \boldsymbol{\omega}_0 = \begin{bmatrix} 0.02 \\ 0.02 \\ 0.01 \end{bmatrix} \text{ rad/s}, \tag{19}$$

where $\boldsymbol{q}_0$ is the initial attitude quaternion, and $\boldsymbol{\omega}_0$ is the initial angular velocity. It is assumed that solar cell currents can be measured on all six sides of the satellite. It is assumed that the cells produce a maximum current of 0.2A when the AM0 irrdiance is perpendicular on the cell surface, and decreases towards zero with the cosine to the angle between the Sun vector and the cell surface normal. The magnetic environment is included in the simulation to obtain three-axis attitude determination. It is assumed that three-axis magnetometer measurements are available on the satellite.

The simulation includes no environmental noise except for the albedo, in order to emphasize the effects of the albedo and albedo correction. The time of the simulation is August 18, 2003, from 11:25:33 to 13:07:11, which is an interval of 101.38 minutes, equivalent to a single orbit. The albedo data used in the simulation of the solar cell currents, are the Earth Probe reflectivity data from August 18th, 2003. The currents i_1 through i_6, induced by the albedo only on each of the six cells are shown in Fig. 9. The bottom plot shows the albedo during the orbit.

From the solar cell currents, i.e. Sun and albedo induced currents, a Sun LOS unit vector is estimated. Since the cells are mounted on a cube, each opposing cell pair, measures the projection of the Sun vector directly on the associated axis of the spacecraft fixed frame (SCB). The SCB frame is centered in the center of mass of the satellite. The true Sun vector and Earth Magnet Field vector, are available in Earth Centered Inertial (ECI) frame from an ephemeris model. The magnetometer measurement is the Earth Magnetic Field vector rotated to the SCB frame. The attitude quaternion representing the attitude of the SCB frame relative to the ECI frame, is calculated using the Q-Method algorithm.[24]

Fig. 10 shows the error in the complex elements of the attitude quaternion calculated by the Q-Method algorithm. The albedo is also shown in the figure, and the correlation between the magnitude of albedo and attitude error, $\boldsymbol{q}_{\text{err}}$, is clear.

The albedo data used to compensate for the albedo are the mean reflectances of 2001, described in Section II. From the albedo model, an estimate of the albedo induced cell currents in Fig. 9 is subtracted from the

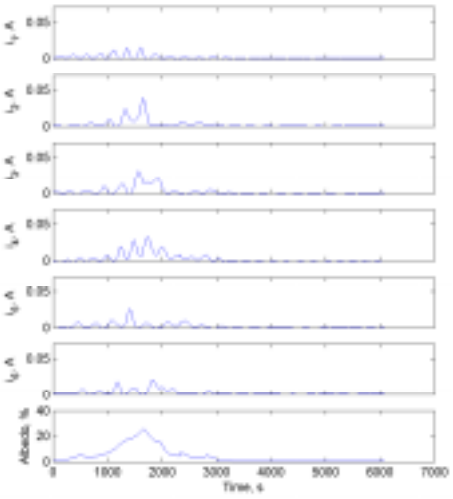

Figure 9. Albedo induced currents on the six solar cells and albedo, during a single orbit of the AAU CubeSat.

measured cell currents. The satellite attitude used in the compensation is the estimated attitude without albedo compensation, i.e. Fig. 10. The albedo corrected cell currents are used to improve the precision of the estimated Sun vector passed to the Q-Method algorithm. The albedo corrected residual error of the satellite attitude quaternion estimate is shown in Fig. 11.

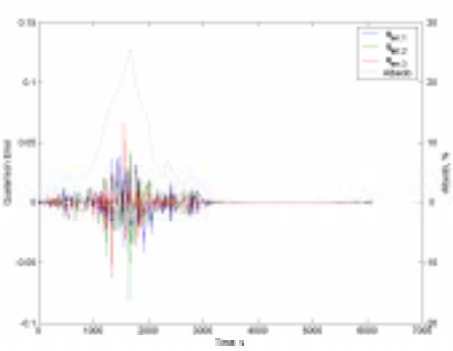

Figure 10. Q-Method algorithm attitude determination error in the complex quaternion elements due to albedo.

By observing Fig. 10 and Fig. 11, it is seen that correcting for the albedo and recalculating the attitude using the Q-Method algorithm, reduces the attitude error significantly. The attitude error is parameterized by the quaternion rotation parameter θ, from the quaternion definition

$$\boldsymbol{q} = \begin{bmatrix} \hat{\boldsymbol{e}} \sin(\theta/2) \\ \cos(\theta/2) \end{bmatrix}, \tag{20}$$

where $\hat{\boldsymbol{e}}$ is the unit vector around which, the rotation of θ is performed. Table D shows the mean $\bar{\theta}$ and standard deviation σ of the error, and the maximum rotation parameter of the attitude error $\theta_{\max}$, with and without albedo compensation. The statistics are calculated only for samples where the albedo is larger than 1%. The mean values are biased, which is expected, since the albedo is significant during only part of the orbit, and deviates the Sun vector estimate in directions defined by the Sun and Earth LOS vectors at these times only. The standard deviation of the error is improved by more than a factor of three from 1.38 deg to 0.45 deg, and the maximum error in the attitude is improved from 9.9 deg to 1.9 deg, when including albedo compensation, which is an improvement of 81%.

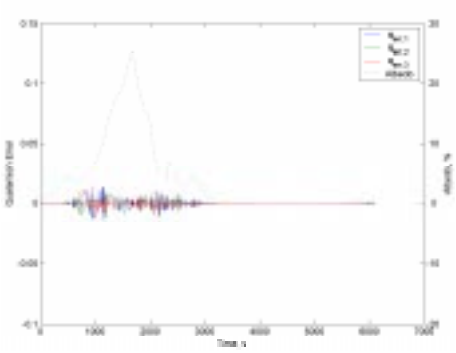

Figure 11. Q-Method algorithm attitude determination error in the complex quaternion elements when applying the albedo to compensate for albedo induced cell currents.

Table 1. Mean, standard deviation, and maximum of the attitude error with and without albedo compensation.

Simulation	$\bar{\theta}$	σ	$\theta_{\max}$
Without albedo compensation	1.54 deg	1.38 deg	9.9 deg
With albedo compensation	0.54 deg	0.45 deg	1.9 deg

IV. Conclusion

A model of the albedo has been derived, based on data from NASA's Total Ozone Mapping Spectrometer. Reflectivity data recorded daily by the Earth Probe Satellite are used to calculate the mean reflectance of Earth. Through detailed calculations of the received radiance of each grid, defined by the reflectivity data, an estimate of the irradiance at the satellite position is estimated.

The mean reflectivity calculated from the Earth Probe data is 30.4%. The results from the albedo model show that the received irradiance by a satellite in vicinity of Earth is dependent on altitude, solar angle, and position over Earth, including both latitude and longitude. The albedo at the 23 deg N latitude is calculated at 90 deg West and Greenwich Meridian. The results show that the albedo at 90 deg West (26.1%) is twice the amount of albedo at 0 deg (13.7%). The albedo at a position over the sunlit boundary is 6.0% at 500km altitude and 5.4% at 800km altitude. Due to the high solar angle to the polar regions, the albedo directly over the poles is between 33.8% and 36.7% even though the reflectivity is in excess of 90%. The maximum albedo is found over Greenland, where the irradiance is 49%. Finally, applying albedo compensation in attitude estimation, improves the maximum error from 9.9 deg to 1.9 deg. The standard deviation is reduced more than a factor three.

A. Future Work

The albedo modeling has been successfully included in the simulation and estimation of satellite systems. However, the model must be verified with actual satellite data. It is the intent of the authors to apply the Ørsted Satellite telemetry to validate the albedo model. Upon validation of the albedo model, a three-axis attitude determination algorithm based solely on solar cell measurements will be presented. The algorithm utilizes the albedo model in order to improve the Sun LOS vector and also estimate the nadir vector. Based on the estimated Sun LOS vector and the nadir, a three-axis attitude can be calculated. Hence, three-axis attitude will be estimated using only solar cells. This algorithm can be combined with other measurements, e.g. from a magnetometer, to improve attitude estimation.

References

[1]Harris, M. and Lyle, R., "Spacecraft Radiation Torques," Tech. Rep. NASA SP-8027, National Aeronautics and Space Administration, October 1969.

[2]Wertz, J. R., editor, *Spacecraft Attitude Determination and Control*, Kluwer Academic Publishers, 1978.

[3]Wertz, J. R., editor, *Mission Geometry: Orbit and Constellation Design and Management*, Microcosm Press AND Kluwer Academic Publishers, 2001.

[4]Psiaki, M. L., Martel, F., and Pal, P. K., "Three-Axis Attitude Determination via Kalman Filtering of Magnetometer Data," *Journal of Guidance, Control, and Dynamics*, Vol. 13, No. 3, May-June 1990, pp. p. 506–514.

[5]van Beusekom, C. J. and Lisowski, R., "Three-Axes Attitude Determination for Falconsat-3," *AIAA Student Conference*, April 2003.

[6]Fisher, H. L., Musser, K. L., and Shuster, M. D., "Coarse attitude determination from Earth albedo measurements," *IEEE Transactions on Aerospace and Electronic Systems*, 1993.

[7]Hales, J. H. and Pedersen, M., "Two-axis MOEMS Sun Sensor for Pico Satellites," *16th Annual AIAA/USU Conference on Small Satelites*, August 2001.

[8]Brasoveanu, D. and Sedlak, J., "Analysis of earth albedo effect on sun sensor measurements based on theoretical model and mission experience," *AAS/GSFC 13th International Symposium on Space Flight Dynamics*, Vol. 1, May 1998, pp. 435–447.

[9]Humphreys, T. E., "Attitude Determination for Small SAtellites with Modest Pointing Constraints," *AIAA Student Conference on Small Satellites*, August 2002.

[10]Aalborg University, http://www.aausatii.aau.dk/, 2004.

[11]Long, M., Lorenz, A., Rodgers, G., Tapio, E., Tran, G., Jackson, K., Twiggs, R., and Bleier, T., "A CubeSat Derived Design for a unique Academic Research Mission in Earthquake Signature Detection," *16th Annual AIAA/USU Conference on Small Satellites*, August 2002.

[12]Swartwout, M., Olsen, T., and Kitts, C., "The Omni-Directional Differential Sun Sensor," *31st Annual International Telemetry Conference: Reengineering Telemetry*, October 1995.

[13]Appel, P., Theil, S., Winkler, S., and Schleicher, A., "Attitude Estimation from Magnetometer and Earth-Albedo-Corrected Coarse Sun Sensor Measurements," *5th International ESA Conference on Spacecraft Guidance, Navigation and Control Systems*, October 2002, pp. 613–616.

[14]Herman, J. R. and Celarier, E. A., "Earth Surface Reflectivity climatology at 240-380nm from TOMS data," *Journal of Geophysical Research*, Vol. 102, No. D23, December 1997, pp. 28003–28011.

[15]Koelemeijer, R. B. A. and Stammes, P., "Potential of GOME for determining the spectral albedo of surfaces - Application to rain forest," *Earth Observation Quarterly*, Vol. 58, March 1998.

[16]Snyder, W. C. and Wan, Z., "BRDF Models to Predict Spectral Reflectance and Emissivity in the Thermal Infrared," *IEEE Transactions On Geoscience and Remote Sensing*, Vol. 36, No. 1, January 1998, pp. 214–225.

[17]Lyle, Robert, Leach, J., and Shubin, L., "Earth Albedo and Emitted Radiation," Tech. Rep. NASA SP-8067, National Aeronautics and Space Administration, July 1971.

[18]Bhanderi, D., http://bhanderi.dk/, 2005.

[19]National Aeronautics and Space Administration, http://jwocky.gsfc.nasa.gov/, 2005.

[20]Mazer, J. A., *Solar Cells: An Introduction to Crystalline Photovoltaic Technology*, Kluwer Academic Publishers, 1997.

[21]Dewitte, S., Joukoff, A., Crommelynck, D., III, R. B. L., Helizon, R., and Wilson, R. S., "Contribution of the Solar Constant (SOLCON) Program to the Long Term Total Solar Irradiance Observations," *Journal of Geophysical Research*, Vol. 106, No. A8, 2001, pp. 15,759.

[22]Emcore, "InGaP/GaAs/Ge Tripple-Junction Solar Cells," Technical specification, EMCORE, 2004.

[23]Ryer, A., *Light Measurement Handbook*, International Light, 1997.

[24]Shuster, M. D. and Oh, S. D., "Three-Axis Attitude Determination from Vector Observations," *Journal of Guidance and Control*, Vol. 4, No. 1, January-February 1981, pp. 70–77.